Chemical Science

Accepted Manuscript

This article can be cited before page numbers have been issued, to do this please use: X. Hu, Y. Wang, H. Liu, J. Wang, Y. Tan, F. Wang, Q. Yuan and W. Tan, *Chem. Sci.*, 2016, DOI: 10.1039/C6SC03401B.

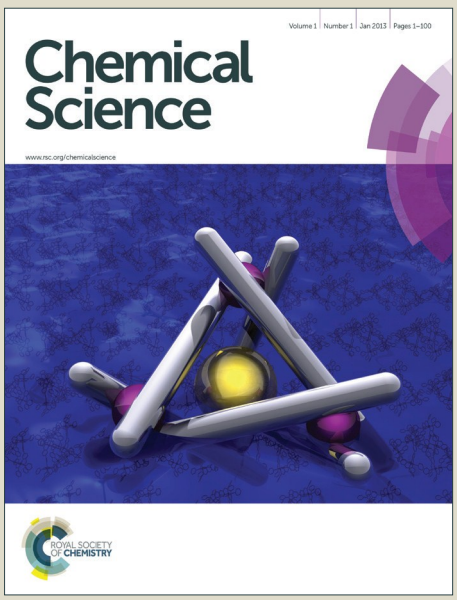

ROYAL SOCIETY OF CHEMISTRY

www.rsc.org/chemicalscience

View Article Online
DOI: 10.1039/C6SC03401B

Journal Name

ARTICLE

Received 00th January 20xx,
Accepted 00th January 20xx

DOI: 10.1039/x0xx00000x

www.rsc.org/

Naked Eye Detection of Multiple Tumor-Related mRNAs from Patients with Photonic-Crystal Micropattern Supported Dual-Modal Upconversion Bioprobes

Xiaoxia Hu,[a] Yingqian Wang,[a] Haoyang Liu,[a] Jie Wang,[a] Yaning Tan,[a] Fubing Wang,[b] Quan Yuan*[a] and Weihong Tan[cd]

Development of a portable device for the detection of multiple mRNAs is a significant need for early diagnosis of cancer. We have designed a biochip-based mRNA detection device combining a hydrophilic–hydrophobic micropattern with upconversion luminescence (UCL) probes. The device achieves highly sensitive detection with the naked eye of multiple mRNAs among patient samples. The high sensitivity is attributed to the enrichment of target concentration and the fluorescence enhancement effect. In addition, since the photonic crystal (PC) dot biochip is functionalized with dual-wavelength excited UCL probes, two kinds of mRNAs in heterogeneous biological samples are detected simultaneously, and the corresponding luminescence signals are captured by an unmodified camera phone. The biochip-based mRNA detection device reported here demonstrates that multiple mRNAs extracted from patient samples can be simultaneously and sensitively detected in a visualized way without sophisticated instrumentation. Therefore, this device is promising in real-time detection of multiple biomarkers in patient samples, and it is anticipated that it will provide a powerful tool for convenient early diagnosis of cancer.

Introduction

Identification of potential cancer biomarkers in patient samples is a key factor in the early diagnosis of cancer.[1–3] The incidence of cancer is closely associated with the abnormal expression of genes, and tumor-related mRNA has been commonly used as a specific biomarker to assess the cancer development stage.[4,5] In recent years, tremendous advances in the field of nucleic acid testing technology offer valuable diagnostic and prognostic approaches for cancer management.[6–12] Among them, use of biochip-based devices for mRNA detection is an emerging assay in clinical diagnostic fields.[13,14] Compared to detection methods in solution systems, biochip-based diagnostics offer the most promising approach for the detection of cancer in point-of-care (POC) applications due to their portability, flexibility, and short sample processing time.[15–17] According to statistics from the article titled "The Worldwide Market For In Vitro Diagnostic (IVD) Tests", the worldwide in vitro diagnostics (IVD) market investment is growing every year, indicating that medical diagnostic tools are playing an increasingly important role in human health assessment and disease diagnosis.[18] The ultimate goal of these endeavors is the development of POC diagnostics having the requisite sensitivity, accuracy, and real-time visualization for patient sample analysis.[13,19] However, most current biochip-based mRNA detection devices cannot simultaneously fulfill these requirements, and no multiplexed biochip has yet shown direct visual detection of multiple mRNAs in patient samples.[20,21] These challenges have limited the clinical application of biochip devices in multiple marker analysis and further impeded their implementation as an effective cancer diagnostic system. Thus, in order to promote the potential clinical utility of such biochip-based devices, more versatile and robust diagnostic devices that satisfy clinical requirements are needed for practical patient sample assay.

Recent innovations in optical detection devices with fluorescence readout have enabled new technological breakthroughs in biomarker analysis.[22–24] However, because of the low concentration of mRNA among crude patient samples, improving the sensitivity of detection devices is an overriding consideration. This can be accomplished in two ways: one is to enrich the target substance from a highly diluted solution to a detectable concentration, and the other is to improve the output signal of the detection device. Taking inspiration from the enrichment phenomena in nature (e.g., beetles collect fog by a hydrophilic–hydrophobic pattern structure on their backs), a strategy for enriching targets from dilute solution is a promising means to raise the analyte concentration.[25,26] Recently, Song and Li have been well demonstrated that the hydrophilic–hydrophobic patterned sensor processed a great ability

[a] Key Laboratory of Analytical Chemistry for Biology and Medicine (Ministry of Education), College of Chemistry and Molecular Sciences, Wuhan University, Wuhan, P. R. China. E-mail: yuanquan@whu.edu.cn
[b] Department of Laboratory Medicine & Center for Gene Diagnosis, Zhongnan Hospital, Wuhan University, Wuhan, P. R. China.
[c] Molecular Science and Biomedicine Laboratory, State Key Laboratory of Chemo/Bio-Sensing and Chemometrics College of Biology and College of Chemistry and Chemical Engineering, Hunan University, Changsha, P. R. China.
[d] Department of Chemistry, Center for Research at the Bio/Nano Interface, Health Cancer Center, UF Genetics Institute, McKnight Brain Institute, University of Florida, Gainesville, USA

† Electronic Supplementary Information (ESI) available: Experimental details and supplementary results. See DOI: 10.1039/x0xx00000x

View Article Online
DOI: 10.1039/C6SC03401B

to enrich target and thus improved the detection sensitivity.[27,28] On the other hand, in order to enhance the output signal of the optical device, fluorescence enhancement can lead to a high signal-to-noise ratio and lower detection limit. Three-dimensional photonic crystals (PCs) are periodic dielectric materials that can confine, control, and manipulate photons.[29–32] They have been frequently used to enhance the intensity of some optical species, thus resulting in hundred-fold enhancement of sensitivity.[27] Overall, by the combined effects of target concentration enrichment and fluorescence enhancement, the sensitivity of mRNA detection among patient samples can be significantly improved.

Cancer is associated with the abnormal expression of multiple tumor-related mRNAs.[33] A diagnostic device with the ability to detect multiple mRNAs simultaneously is required to avoid false positive results, thus improving the reliability of early cancer diagnosis.[34] Lanthanide-doped upconversion nanoparticles (UCNPs) that convert near-infrared (NIR) excitation light into shorter wavelength luminescence have recently been widely used as biological probes due to their unique optical properties, such as the absence of autofluorescence, greater light penetration depths and high resistance to photobleaching.[35–37] However, while UCNPs can afford tunable multicolor upconversion luminescence (UCL) by controlling the lanthanide ion dopants, they typically cause color crosstalk using the same excitation wavelength,[38,39] which limits the sensitivity and accuracy of multi-analyte detection. Most recently, as an exciting new class of nanophosphors that convert 808 nm NIR light into shorter wavelength luminescence, Nd^{3+} ion-doped UCNPs have attracted great attention for biosensing and imaging.[40–42] Simultaneous detection of multiple mRNAs can be readily realized by the combination of 808 nm and 980 nm excited UCNPs to avoid color crosstalk between different labelling signals and allow visual detection to be achieved.

In this work, a biochip-based mRNA detection device with a hydrophilic–hydrophobic micropattern is designed to achieve highly accurate and sensitive detection of multiple mRNAs among patient samples with the naked eye. This portable visual technique provides a powerful tool for convenient cancer diagnosis by fixing two kinds of specific UCNP-based mRNA probes on the PC substrates. Our novel mRNA detection device can achieve sensitive, visual detection of multiple mRNAs. The excellent performance of our mRNA detection device can lead to further development into a clinical diagnostic device. This strategy can be extended to design a universal detection device, and it is anticipated that this general method will find wide-range applications in the area of health assessment and disease diagnosis.

Results and discussion

We sought to generate an mRNA detection device for sensitive bioanalysis of mRNA that is (i) straightforward to fabricate, (ii) sensitive when presented with heterogeneous biological samples, and (iii) convenient for reading the assay result without any major instrumentation. To satisfy these requirements, a PC dots-based substrate was fabricated by depositing hydrophilic PC dots on a hydrophobic surface. As illustrated in Fig. 1a, aqueous colloidal droplets containing carboxyl-modified polystyrene spheres are

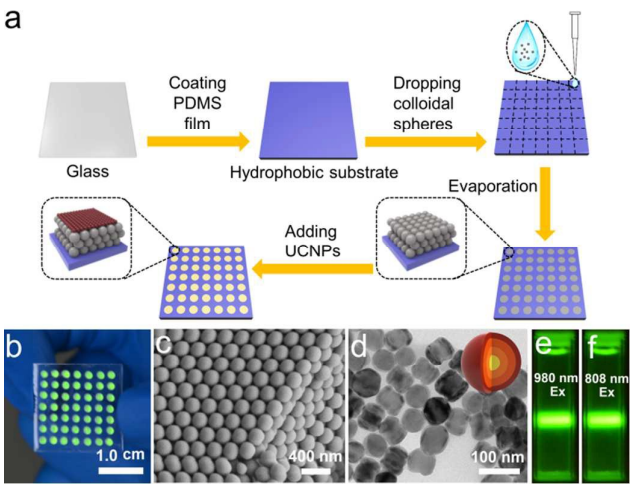

Fig. 1 (a) Schematic illustration of fabricating a PC dots-based substrate. (b) Photograph of the PC-based substrate under exposure to sunlight. (c) SEM image of the PC dots. (d) TEM image of the Er-doped UCNPs. Inset: the structure of the core-shell structured UCNPs. Luminescence photograph of the Er-doped UCNPs with 980 nm (e) and 808 nm (f) illumination at excitation power density of 1.00 W/cm^2. The Er-doped UCNPs are dispersed in water.

dropped onto the specific planning area of the hydrophobic PDMS substrate. Then, concentration leads to the formation of macroscopic PC dots during solvent evaporation, and finally UCNPs are added to the PC dots. As shown in Fig. 1b, aqueous colloidal droplets were regularly assembled into an orderly PC dot array, which appeared green due to the Bragg scattering effect, *via* an evaporation-induced procedure on the hydrophobic substrate. Scanning electron microscopy (SEM) demonstrated that the PC dot array was regularly assembled from the monodispersed PS spheres (Fig. 1c) with diameters of 215 nm (Fig. S1†). To fabricate efficient optical probes, the core-shell structured β-$NaYF_4$:Yb,Er@$NaYF_4$:Yb@$NaNdF_4$:Yb@$NaYF_4$:Yb (denoted as Er-doped UCNPs) possessing dual NIR excitations (808 nm and 980 nm) and the core-shell structured β-$NaYF_4$:Yb,Tm@$NaYF_4$:Yb (denoted as Tm-doped UCNPs) were employed as light-emitting materials.[43] The transmission electron microscopy (TEM) images (Fig. 1d and Fig. S2†) and the size distribution statistics (Fig. S3†) indicated that the Er-doped UCNPs were constructed by epitaxial layer by layer growth and the as-prepared core-shell UCNPs exhibited uniform sizes with diameters of approximately 65 nm. The TEM images (Fig. S4†) of the Tm-doped UCNPs showed that the nanoparticles had well-defined hexagonal shapes, and the mean diameter was found to be approximately 60 nm (Fig. S5†). X-ray powder diffraction (XRD) patterns of Er-doped UCNPs (Fig. S6†) and Tm-doped UCNPs (Fig. S7†) showed that the diffraction lines were ascribed to the hexagonal structure of $NaYF_4$ with positions and intensities of the peaks in good agreement with the calculated values for hexagonal-$NaYF_4$. Upconversion properties were examined using continuous wave (CW) laser excitation at 980 nm

View Article Online
DOI: 10.1039/C6SC03401B

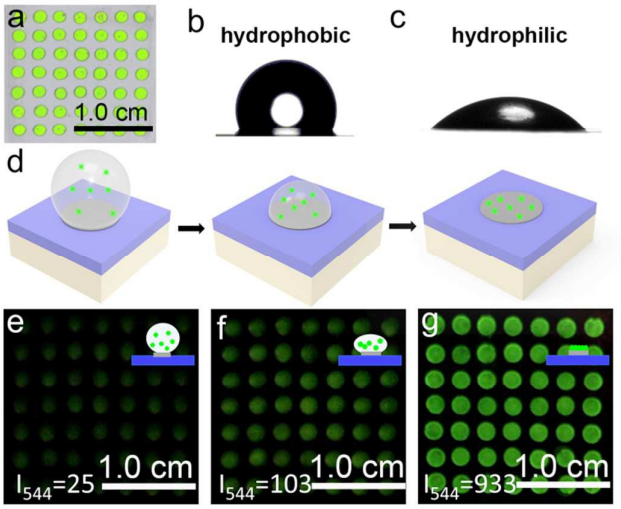

Fig. 2 (a) Photograph of the PC dot micropattern with hydrophilic PC dots on the hydrophobic PDMS surface. (b & c) Contact angle characterization of the PDMS-based hydrophobic surface (b) and PC dot substrate (c). (d) Illustration of the gradual enrichment process of UCNPs from the highly diluted solution to the PC dot arrays. (e–g) Luminescence images of the PC dot micropattern with UCNP solution during the condensing-enrichment process with 808 nm illumination at excitation power density of 0.50 W/cm^2. Inset: sketch of the condensed state.

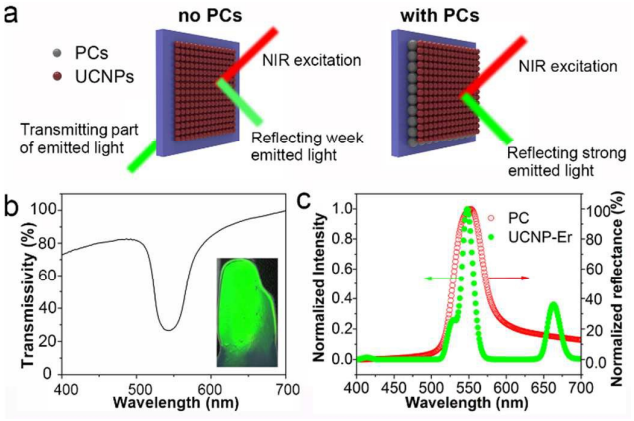

Fig. 3 (a) The optical pathway diagram of the upconversion emitted light when Er-doped UCNPs are deposited on the substrate without (left) and with (right) PCs under NIR excitation. (b) Transmittance spectrum of the PC film. Inset: photograph of the PC film. (c) Reflection spectrum of PC film, together with the normalized luminescence spectrum of the Er-doped UCNPs dispersed in water under 808 nm excitation.

and 808 nm. As shown in Fig. 1e and Fig. 1f, in both cases, the Er-doped UCNPs gave intense green luminescence when they were doped with Nd^{3+} ion. Remarkably, due to the efficient suppression of surface-related deactivation, a large enhancement of the upconversion luminescence (UCL) was obtained after simply coating the outmostshell (Fig. S8† and Fig. S9†), which could promote efficient upconversion emission for imaging applications. The Tm-doped UCNPs showed blue emission band at 477 nm using CW laser excitation at 980 nm (Fig. S10†).

The PC dot micropattern was fabricated by assembling hydrophilic PC dots on a PDMS hydrophobic substrate. The colloidal solution containing monodispersed PS spheres self-assembled into a regular array on the hydrophobic surface and showed a bright green color when exposed to sunlight (Fig. 2a). The PDMS-coated glass displayed highly hydrophobic behavior with a contact angle of 117.3° ± 2.3° (Fig. 2b), while the contact angle of the PC dot array was 32.3° ± 2.1° and resulted in a hydrophilic surface (Fig. 2c). Because of the different wettability between the PDMS-based substrate and PC dots, the highly diluted solution of substances could condense onto the hydrophilic PC dots. As illustrated in Fig. 2d, the solution of UCNPs is first dropped on the PC dots. With the evaporation of water, the solution dewet from the hydrophobic substrate and UCNPs are condensed on the PC dots. Herein, the images of luminescence intensities were clearly obtained using an unmodified camera phone. At the beginning, the luminescence image of UCNPs deposited on PC dots was dark due to the highly diluted solution of UCNPs (Fig. 2e), and then the UCL intensity increased after the evaporation of part of the water (Fig. 2f). When the water dried, the UCNPs deposited on PC dots became much brighter due to complete enrichment of the UCNPs (Fig. 2g). The corresponding luminescence spectra of per PC dot also showed that the visible emission light of PC dots became brighter and brighter during the enrichment process (Fig. S11†). Compared to the UCL intensity of UCNPs on a PC dot, the luminescence intensity of a droplet containing the same number of UCNPs on a pure hydrophilic PC film after evaporation declined by half (Fig. S12†), which further confirmed the great enrichment ability of the PC dots-based substrate with hydrophilic–hydrophobic pattern.

Due to their photonic band-gap property, three-dimensional PC material can be used to modulate the emission wavelength and intensity of optical species.[44] In particular, enhanced luminescence can be obtained when UCNPs are combined with PCs because of the enhanced reflection of emitted light.[45] As illustrated in Fig. 3a, without PCs, only part of emitted light of UCNPs can be reflected and most is transmitted through the glass substrate, thus the luminescence of UCNPs is not enhanced. However, when the glass substrate is coated with PC dots, almost all of emitted light is reflected. Since the PCs can efficiently prevent the emitted light from being transmitted through the substrate, the luminescence signal of UCNPs is readily enhanced. As shown in the transmittance spectrum in Fig. 3b, the stopband of the PC film was located at 552 nm. The inset image in Fig. 3b presented green color under exposure to sunlight duo to the Bragg scattering effect. Also, as shown in Fig. 3c, the reflection spectrum of the PC film showed the stopband centered at 552 nm. Er-doped UCNPs showed a green emission band at 544 nm under NIR excitation, which overlapped well with the stopband of PC. This result indicates that the photonic gap of PCs can efficiently reflect the green emission band at 544 nm

View Article Online
DOI: 10.1039/C6SC03401B

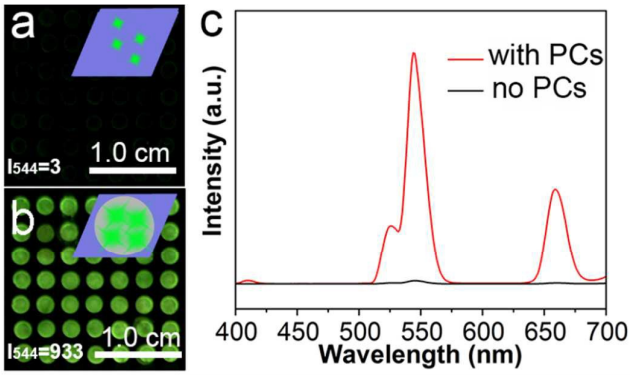

Fig. 4 Luminescence images of the Er-doped UCNPs deposited on the substrates without (a) and with (b) PC dots at excitation power density of 0.50 W/cm^2 of 808 nm light. Inset: illustration of the UCNPs deposited on the substrate. (c) UCL spectra of the Er-doped UCNPs on the substrate with and without PCs. I_{544} is the UCL intensity of the emission band at 544 nm.

and prevent transmission of the emitted light, leading to an enhancement of the UCL.

The enhancement ability of the PC dot for UCNPs was investigated by comparing the luminescence intensities of UCNPs on different substrates: substrate without PC dots and substrate with PC dots. It can be noted that the luminescence image in Fig. 4a was dark as there was no PC dot on the substrate. However, when UCNPs were loaded on the substrate with PC dots, the luminescence image became bright (Fig. 4b). The enhanced luminescence intensity of UCNPs was attributed to the optical enhancement effect of the PCs. These captured luminescence photographs clearly suggest that the PC dot substrate displays a powerful ability to enhance the luminescence of UCNPs. The corresponding luminescence spectra (Fig. 4c) also showed that the luminescence intensity of the UCNPs on the PC dot substrate was much stronger than that on the substrate without PCs. These results prove that the PC dot substrate is an efficient tool for enhancing the luminescence intensity of UCNPs.

According to previous studies, mRNAs are proposed to be important markers for tumor growth and they are usually chosen to assess the stage of cancer development.[46] However, it is reported that a specific kind of tumor may correlate with multiple mRNA markers, and some tumor-related mRNAs are also expressed in normal tissues. Thus, if more than one kind of tumor-related mRNA exists, the diverse expression levels of these mRNAs should all be detected to improve the reliability of diagnosis. Fig. 5a illustrates the construction of a flexible device for the simultaneous detection of multiple tumor biomarkers. Specifically, different kinds of UCNP-based probes (two probes named probe 1 and probe 2 are taken as an example) are constructed by labelling the recognition sequences of different target mRNAs (target 1 and target 2 are taken as an example) with Er-doped UCNPs (λexc = 808 nm, λem = 544 nm) and Tm-doped UCNPs (λexc = 980 nm, λem = 477 nm), respectively. The detection device is composed of the PC dot substrate, UCNP-based probes and graphene oxide (GO). The UCNP-based probes are immobilized on the PC dot substrate and then bind to GO *via* π–π stacking between the nucleobases of recognition sequences and sp^2 bonded carbon atoms of GO. The detection of two kinds of mRNAs with the above device is illustrated in Fig. 5b and Fig. S14a†. When neither target is present, the luminescence is very weak due to the quenching of UCL by GO. In the presence of two targets, the two kinds of probes hybridize with their corresponding targets, leading to the recovery of the luminescence signal due to the detachment of GO from the two kinds of probes. In the presence of one kind of target, only the corresponding probe hybridizes with the target and its luminescence signal recovers. Previous studies reported that TK1 mRNA and C-myc mRNA were highly correlated with the development of breast cancer,[43] thus these two kinds of mRNAs were chosen to test the biosensing capabilities of the device. In the presence of GO, the UCL at 477 nm and 544 nm of decreased

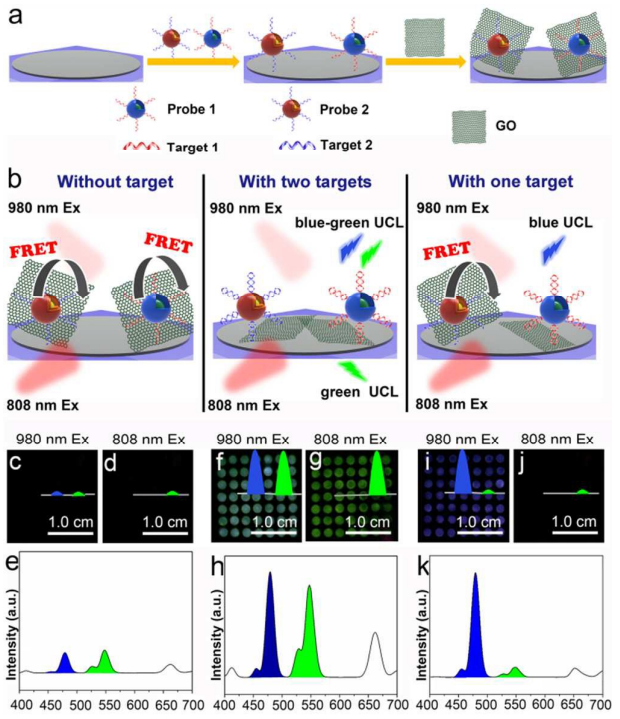

Fig. 5 (a) Schematic illustration of the construction of a flexible detection device. (b) Working principle for the simultaneous detection of multiple mRNAs. (c & d) Luminescence images of the biochip-based detection device without mRNAs using 980 nm (c) and 808 nm (d) excitation. Insets: diagrams of UCL bands at 477 and 544 nm. (e) UCL spectrum of the detection device without mRNAs. (f & g) Luminescence images of the detection device with the addition of TK1 and C-myc mRNAs using 980 nm (f) and 808 nm (g) excitation. Insets: diagrams of UCL bands at 477 and 544 nm. (h) UCL spectrum of the detection device with the addition of TK1 and C-myc mRNAs. (i & j) Luminescence images of the detection device when only C-myc mRNA was present using 980 nm (i) and 808 nm (j) excitation. Insets: diagrams of UCL bands at 477 and 544 nm. (k) UCL spectrum of the detection device with the addition of only C-myc mRNA. The excitation power density of 980 nm and 808 nm CW laser is 0.50 W/cm^2.

View Article Online
DOI: 10.1039/C6SC03401B

gradually with 980 nm excitation, indicating the UCL can be effectively quenched by GO (Fig. S13†). The luminescence images of the detection device without mRNA added were dark with both 980 nm (Fig. 5c) and 808 nm (Fig. 5d) excitation due to the weak visual emission bands at 477 nm and 544 nm (Fig. 5e). With the simultaneous addition of TK1 mRNA and C-myc mRNA, the device exhibited blue-green luminescence consisting of green and blue bands with 980 nm laser illumination (Fig. 5g). The UCL spectrum with excitation at 980 nm showed that the luminescence intensities at both 477 nm and 544 nm were enhanced when the two kinds of mRNAs were present simultaneously (Fig. 5h). When only one kind of mRNA target (e.g., C-myc mRNA) was present, the device emitted blue luminescence with excitation at 980 nm (Fig. 5i). The test zone became dark when the wavelength of CW laser was changed to 808 nm, since the UCL of Tm-doped UCNPs cannot be excited at 808 nm (Fig. 5j). The corresponding luminescence spectrum also demonstrated that only the blue luminescence triggered by C-myc mRNA was observed (Fig. 5k). Similarly, in the presence of only TK1 mRNA, the detection device exhibited green luminescence under both 980 nm (Fig. S14b†) and 808 nm (Fig. S14c†) excitation because the Er-doped UCNPs can be excited at both 980 nm and 808 nm. As a result, this mRNA detection device exhibited good selectivity for simultaneous detection of two kinds of mRNAs. In addition, the UCL intensity of PC dots was gradually weakened when the concentrations of TK1 mRNA and C-myc mRNA were decreased from 0.1 nM to 0.01 nM and the detection limit was determined to be 0.01 nM (Fig. S15† and Fig. S16†), demonstrating that the detection device also exhibited high sensitivity for detection of mRNAs. The luminescence from the mRNA detection device was visible with the naked eye and could be captured by an unmodified camera phone. The above results therefore indicated that the mRNA detection device was capable of simultaneous and sensitive detection of multiple mRNAs with the naked eye.

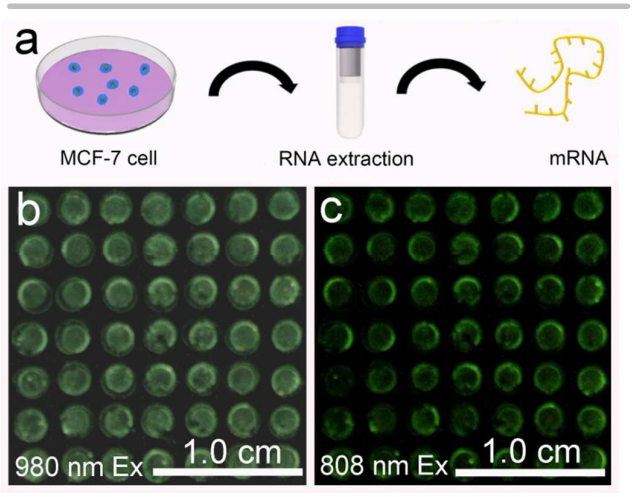

Fig. 6 (a) Schematic illustration of the mRNA extraction from MCF-7 cell. The luminescence images of the mRNA detection devices with the addition of targets extracted from MCF-7 cell with 980 nm (b) and 808 nm (c) illumination at excitation power density of 0.50 W/cm^2.

The favourable performance of the mRNA detection device indicated a promising prospect for assay of mRNAs present in heterogeneous biological samples. MCF-7 cell is a human breast adenocarcinoma cell line, where TK1 and C-myc mRNAs are all overexpressed. mRNAs isolated from MCF-7 cells were detected to preliminarily determine whether the device was robust for analysis of biological samples (Fig. 6a). In the presence of mRNAs extracted from 10^5 MCF-7 cells, the device exhibited blue-green luminescence consisting of green and blue bands with 980 nm laser illumination (Fig. 6b). In addition, the device exhibited green luminescence under 808 nm excitation (Fig. 6c). The luminescence spectra showed that in comparison to the UCL intensity of the device without mRNA extracts, stronger visual emission bands at 477 nm and 544 nm were obtained under 980 nm excitation when there existed mRNAs extracted from MCF-7 cells (Fig. S17†). The mRNA detection device is therefore highly sensitive for the detection of crude biological samples.

To investigate the applicability of this device in clinical diagnosis, mRNAs extracted from breast cancer patient samples were further assayed. Since expression levels of certain mRNAs are accurate predictors of the patient's overall prognosis, mRNAs from breast cancer tissues were extracted to investigate the expression level of corresponding mRNAs, as shown in Fig. 7a. Also, mRNAs from corresponding non-cancerous normal tissues of the same patient were extracted. As show in Fig. 7b, three breast cancer patient samples containing cancer tissues and corresponding non-cancerous normal tissues were detected simultaneously. The detection device without RNA extracts was employed as a blank, and it showed dark images using 980 nm laser illumination. When there were mRNAs extracted from normal tissues, the luminescence images of the detection devices were slightly brighter

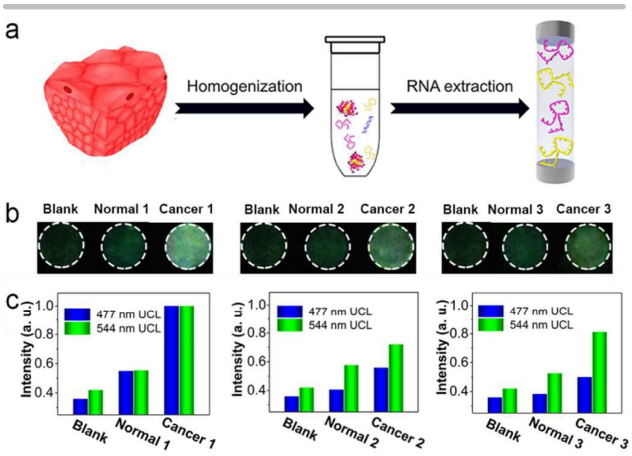

Fig. 7 (a) Schematic illustration of the mRNA extraction from patient samples. (b) Luminescence images of the mRNA detection devices with 980 nm illumination at excitation power density of 0.50 W/cm^2. Blank: without RNA extracts. Normal: with RNA extracts from normal tissue. Cancer: with RNA extracts from cancer tissue. (c) The luminescence intensities of the mRNA detection devices with the addition of three patient samples containing normal tissues and cancer tissues.

View Article Online
DOI: 10.1039/C6SC03401B

than the blank group, indicating normal tissue expressed low levels of TK1 and C-myc mRNA. Furthermore, in the presence of mRNAs extracted from breast cancer tissues, the detection areas on the devices all exhibited bright blue-green luminescence consisting of green and blue luminescence bands using 980 nm laser illumination. Clearly, with the addition of mRNAs extracted from breast cancer tissues, the detection devices exhibited significantly much stronger luminescence than the groups with mRNAs extracted from normal tissues, and these effects were detected by the naked eye. It can be clearly noted that similar results were obtained when three patient samples were assayed simultaneously, demonstrating that TK1 mRNAs and C-myc mRNAs were all overexpressed in breast tumor tissue, but expressed at relatively low levels in normal tissue. The corresponding luminescence spectra of the detection devices were further obtained, as shown in Fig. 7c, and the UCL intensities from the breast cancer tissues were much higher than those of the normal tissues and the blank group. These results demonstrate that our device holds great promise for cancer diagnostics.

Conclusions

In conclusion, the new mRNA detection device described here was able to read tumor-related mRNAs directly in clinically relevant samples using luminescence signals of UCNPs for the first time. The biochip-based mRNA detection device with a hydrophilic–hydrophobic pattern showed both target enrichment ability and luminescence enhancement simultaneously, thus leading to sensitive detection of mRNAs extracted from patient samples with the naked eye. More importantly, since distinct excitation-emission peaks were obtained using irradiation by two CW lasers at wavelengths of 980 nm and 808 nm, the detection device exhibited good accuracy for the simultaneous detection of two kinds of mRNAs, and successfully avoided false positive results. The results of luminescence images captured by an unmodified camera phone proved that such a detection device was capable of assaying patient samples without sophisticated instrumentation. This multifunctional device shows great potential for early diagnosis of cancer and is anticipated to find extensive applications in clinical diagnosis and life science.

Acknowledgements

This work was supported by the National Natural Science Foundation of China (51272186, 21422105), A Foundation for the Author of National Excellent Doctoral Dissertation of PR China (201220), Ten Thousand Talents Program for Young Talents, the Fundamental Research Funds for the Central Universities (2015203020207), and the Fund Program of Health and Family Planning Commission of Hubei Province (WJ2015MB032). Q. Yuan thanks the large-scale instrument and equipment sharing foundation of Wuhan University.

Notes and references

1 L. Wu and X. G. Qu, *Chem. Soc. Rev.*, 2015, **44**, 2963–2997.
2 N. Karachaliou, C. Mayo-de-las-Casas, M. A. Molina-Vila and R. Rosell, *Ann. Transl. Med.*, 2015, **3**, 36.
3 N. Li, C. Y. Chang, W. Pan and B. Tang, *Angew. Chem. Int. Ed.* 2012, **51**, 7426–7430; *Angew. Chem.*, 2012, **124**, 7544–7548.
4 D. Hanahan and R. A. Weinberg, *Cell*, 2000, **100**, 57–70.
5 X. H. Peng, Z. H. Cao, J. T. Xia, G. W. Carlson, M. M. Lewis, W. C. Wood and L. Yang, *Cancer Res.*, 2005, **65**, 1909–1917.
6 D. S. Seferos, D. A. Giljohann, H. D. Hill, A. E. Prigodich and C. A. Mirkin, *J. Am. Chem. Soc.*, 2007, **129**, 15477–15479.
7 A. Raj, P. Bogaard, S. A Rifkin, A. Oudenaarden and S. Tyagi, *Nat. Methods*, 2008, **5**, 877–879.
8 M. H. Lin, J. J. Wang, G. B. Zhou, J. B. Wang, A. Wu, J. X. Lu, J. M. Gao, X. Q. Chen, J. Y. Shi, X. L. Zuo and C. H. Fan, *Angew. Chem. Int. Ed.*, 2015, **54**, 2151–2155; *Angew. Chem.*, 2015, **127**, 2179–2183.
9 L. P. Qiu, C. C. Wu, M. X. You, D. Han, T. Chen, G. Z. Zhu, J. H. Jiang, R. Q. Yu and W. H. Tan, *J. Am. Chem. Soc.*, 2013, **135**, 12952–12955.
10 A. R. Buxbaum, B. Wu and R. H. Singer, *Science*, 2014, **343**, 419–422.
11 R. X. Duan, X. L. Zuo, S. T. Wang, X. Y. Quan, D. L. Chen, Z. F. Chen, L. Jiang, C. H. Fan and F. Xia, *J. Am. Chem. Soc.*, 2013, **135**, 4604–4607.
12 K. Zhang, X. Zhu, F. Jia, E. Auyeung and C. A. Mirkin, *J. Am. Chem. Soc.*, 2013, **135**, 14102–14105.
13 N. W. Choi, J. Kim, S. C. Chapin, T. Duong, E. Donohue, P. Pandey, W. Broom, W. A. Hill and P. S. Doyle, *Anal. Chem.*, 2012, **84**, 9370–9378.
14 Y. Wu, K. J. Kwak, K. Agarwal, A. Marras, C. Wang, Y. Mao, X. Huang, J. Ma, B. Yu, R. Lee, A. Vachani, G. Marcucci, J. C. Byrd, N. Muthusamy, G. Otterson, K. Huang, C. E. Castro, M. Paulaitis, S. P. Nana-Sinkam and L. J. Lee, *Anal. Chem.*, 2013, **85**, 11265–11274.
15 L. Gervais, N. de Rooij and E. Delamarche, *Adv. Mater.*, 2011, **23**, H151–H176.
16 S. K. Vashist, E. Lam, S. Hrapovic, K. B. Male and J. H. T. Luong, *Chem. Rev.*, 2014, **114**, 11083–11130.
17 Y. Bourquin, A. Syed, J. Reboud, L. C. Ranford-Cartwright, M. P. Barrett and J. M. Cooper, *Angew. Chem. Int. Ed.*, 2014, **53**, 5587–5590; *Angew. Chem*., 2014, **126**, 5693–5696.
18 *The Worldwide Market For In Vitro Diagnostic (IVD) Tests, 6th Edition [with 2009 Economy Preface]: Kalorama Information,* 2008.
19 A. Sassolas, B. D. Leca-Bouvier and L. J. Blum, *Chem. Rev.*, 2008, **108,** 109–139.
20 Z. Fang, L. Soleymani, G. Pampalakis, M. Yoshimoto, J. A. Squire, E. H. Sargent and S. O. Kelley, *ACS Nano*, 2009, **3**, 3207–3213.
21 Y. H. Liu, H. X. Yao and J. Zhu, *J. Am, Chem. Soc.*, 2013, *135*, 16268.
22 C. McDonagh, C. S. Burke and B. D. MacCraith, *Chem. Rev.*, 2008, **108**, 400–422.
23 J. R. Manzano, M. A. Karymov, S. Begolo, D. A. Selck, D. V. Zhukov, E. Jue and R. F. Ismagilov, *ACS Nano*, 2016, **10**, 3102–3113.
24 W. W. Chen, Q. Z. Li, W. S. Zheng, F. Hu, G. X. Zhang, Z. Wang, D. Q. Zhang and X. Y. Jiang, *Angew. Chem. Int. Ed.*, 2014, **53**, 13734–13739; *Angew. Chem. Int. Ed.*, 2014, **126**, 13954–13959.
25 A. R. Parker and C. R. Lawrence, *Nature*, 2001, **414**, 33–34.
26 T. Darmanin and F. Guittard, *J. Mater. Chem., A* 2014, *2*, 16319.
27 J. Hou, H. Zhang, Q. Yang, M. Li, Y. Song and L. Jiang, *Angew. Chem. Int. Ed.*, 2014, **53**, 5791–5795; *Angew. Chem.*, 2014, **126**, 5901–5905.
28 J. Hou, H. C. Zhang, Q. Yang, M. Z. Li, L. Jiang and Y. L. Song, *Small,* 2015, **11**, 2738–2742.
29 E. Yablonovitch, *Phys. Rev. Lett.*, 1987, **58**, 2059–2062.
30 A. Scherer, O. Painter, J. Vuckovic, M. Loncar and T. Yoshie, *IEEE Trans. Nanotechnol.*, 2002, **1**, 4–11.
31 W. Z. Shen, M. Z. Li, L. A. Xu, S. T. Wang, L. Jiang, Y. L. Song and D. B. Zhu, *Biosens. Bioelectron.*, 2011, **26**, 2165–2170.
32 M. Z. Li, F. He, Q. Liao, J. Liu, L. Xu, L. Jiang, Y. L. Song, S. Wang

View Article Online
DOI: 10.1039/C6SC03401B

and D. B. Zhu, *Angew. Chem. Int. Ed.*, 2008, **47**, 7258–7262; *Angew. Chem.*, 2008, **120**, 7368–7372.
33 D. Sidransky, *Science*, 1997, **278**, 1054–1058.
34 L. Zhou, R. Wang, C. Yao, X. Li, C. Wang, X. Zhang, C. Xu, A. Zeng, D. Zhao and F. Zhang, *Nat. Commun.*, 2015, **6**, 6938.
35 M. Haase and H. Schafer, *Angew. Chem. Int. Ed.*, 2011, **50**, 5808–5829; *Angew. Chem.*, 2011, **123**, 5928–5950.
36 J. Liu, Y. Liu, Q. Liu, C. Li, L. Sun and Y. F. Li, *J. Am. Chem. Soc.*, 2011, **133**, 15276–15279.
37 G. Chen, H. Qiu, P. N. Prasad and X. Y. Chen, *Chem. Rev.*, 2014, **114**, 5161–5214.
38 G. Tian, Z. Gu, L. Zhou, W. Yin, X. Liu, L. Yan, S. Jin, W. Ren, G. Xing, S. Li and Y. Zhao, *Adv. Mater.*, 2012, **24**, 1226–1231.
39 S. Wu, N. Duan, Z. Shi, C. Fang and Z. Wang, *Anal. Chem.*, 2014, **86**, 3100–3107.
40 X. Xie, N. Gao, R. Deng, Q. Sun, Q. H. Xu and X. G. Liu, *J. Am. Chem. Soc.*, 2013, **135**, 12608–12611.
41 Y. F. Wang, G. Y. Liu, L. D. Sun, J. W. Xiao, J. C. Zhou and C. H. Yan, *ACS Nano*, 2013, **7**, 7200–7206.
42 X. Li, Z. Guo, T. Zhao, Y. Lu, L. Zhou, D. Zhao and F. Zhang, *Angew. Chem. Int. Ed.*, 2016, **55**, 2464–2469; *Angew. Chem.*, 2016, **128**, 2510–2515.
43 B. Liu, Y. Y. Chen, C. X. Li, F. He, Z. Y. Hou, S. S. Huang, H. M. Zhu, X. Y. Chen and J. Lin, *Adv. Funct. Mater.*, 2015, **25**, 4717–4729.
44 Z. Yin, Y. S. Zhu, W. Xu, J. Wang, S. Xu, B. Dong, L. Xu, S. Zhang and H. W. Song, *Chem. Commun.*, 2013, **49**, 3781–3783.
45 J. L. Liao, Z. W. Yang, H. J. Wu, D. Yan, J. B. Qiu, Z. G. Song, Y. Yang, D. C. Zhou and Z. Y. Yin, *J. Mater. Chem. C,* 2013, **1**, 6541–6546.
46 J. F. R. Robertson, K. L. ONeill, M. W. Thomas, P. G. McKenna and R. W. Blamey, *Br. J. Cancer,* 1990, **62**, 663–667.